

COOLING RATE DEPENDENCE AND DYNAMIC HETEROGENEITY BELOW THE GLASS TRANSITION IN A LENNARD-JONES GLASS

K. Vollmayr-Lee¹, W. Kob², K. Binder² and A. Zippelius³

¹*Department of Physics, Bucknell University,
 Lewisburg, PA 17837, USA*

and

²*Institute of Physics, Johannes-Gutenberg-University Mainz
 Staudinger Weg 7, 55099 Mainz, Germany*

and

³*Institute of Theoretical Physics, Georg-August-University Göttingen
 Bunsenstr.9, 37073 Göttingen, Germany*

We investigate a binary Lennard-Jones mixture with molecular dynamics simulations. We consider first a system cooled linearly in time with the cooling rate γ . By varying γ over almost four decades we study the influence of the cooling rate on the glass transition and on the resulting glass. We find for all investigated quantities a cooling rate dependence; with decreasing cooling rate the system falls out of equilibrium at decreasing temperatures, reaches lower enthalpies and obtains increasing local order. Next we study the dynamics of the melting process by investigating the most immobile and most mobile particles in the glass. We find that their spatial distribution is heterogeneous and that the immobile/mobile particles are surrounded by denser/less dense cages than an average particle.

1. Introduction

If a liquid is cooled rapidly enough it avoids crystallization and falls out of equilibrium. The resulting system is in an amorphous state and shows dramatically different dynamics than the high temperature liquid.¹ Computer simulations provide access to microscopic information of these interesting static and dynamic features.

In this paper we will present molecular dynamics simulations of a binary Lennard-Jones mixture which has been shown to be not prone to crystallization.² Our goal is to investigate both the influence of the cooling rate on the statics of the glass, as well as the dynamics of melting as the glass is heated.

The outline of this paper is as follows. In the next section we present the interaction model and details of the simulation. In section 3 we investigate the cooling rate dependence, first by studying the influence of the cooling rate on the cooling process, i.e. the glass transition, and second, by investigating the resulting end

configurations and the microscopic origin of the cooling rate dependence. More extensive reports can be found elsewhere³, as well as similar cooling rate studies for amorphous silica⁴. In section 4 we investigate the dynamics of a melting process via the spatial distribution and the surrounding of the fastest and the slowest particles *below* the glass transition (similar to the work of Kob *et al.*⁵ *above* the glass transition). We finish with a summary.

2. Model and Details of the Simulation

We use a binary Lennard-Jones mixture where the two particle types, A and B, have the same mass m . The interaction potential for particles i and j at positions \vec{r}_i and \vec{r}_j and of type $\alpha, \beta \in \{\text{A,B}\}$ is

$$V_{\alpha\beta}(r) = 4\epsilon_{\alpha\beta} \left(\left(\frac{\sigma_{\alpha\beta}}{r} \right)^{12} - \left(\frac{\sigma_{\alpha\beta}}{r} \right)^6 \right), \quad (2.1)$$

where $r = |\vec{r}_i - \vec{r}_j|$. To avoid crystallization the potential parameters are chosen to be $\epsilon_{\text{AA}} = 1.0$, $\epsilon_{\text{AB}} = 1.5$, $\epsilon_{\text{BB}} = 0.5$, $\sigma_{\text{AA}} = 1.0$, $\sigma_{\text{AB}} = 0.8$ and $\sigma_{\text{BB}} = 0.88$.² We use reduced units: the unit of length is σ_{AA} , the unit of energy is ϵ_{AA} and the unit of time is $\sqrt{m\sigma_{\text{AA}}^2/48\epsilon_{\text{AA}}}$. For the molecular dynamics simulations we use the velocity Verlet algorithm with a step size $\Delta t = 0.02\tau$. All simulations are done with 800 A and 200 B particles. To get better statistics all quantities are averaged over 10 configurations.

For section 3 we use the constant pressure algorithm proposed by Andersen⁶ with the piston mass $M = 0.05$ and the external pressure $p_{\text{ext}} = 0$. For section 4 the microcanonical ensemble is used.

3. Cooling Rate Dependence

In this section we investigate how the glass transition and the resulting glass depend on its history. In specific, we cool the system from a high temperature, $T_0 = 2.0$, to zero temperature by coupling it to a stochastic heat bath. The bath temperature T_b is decreased linearly in time t with the cooling rate γ , i.e.

$$T_b(t) = T_0 - \gamma t. \quad (3.1)$$

We simulated 13 different cooling rates, ranging from $\gamma = 0.02$ to $\gamma = 3.125 \cdot 10^{-6}$.

3.1. Glass Transition

Here we investigate the system during the cooling process. In Fig. 1 we show the enthalpy $H = U_{\text{pot}} + U_{\text{kin}} + \frac{M}{2}\dot{V}^2 + p_{\text{ext}}V$ as a function of the heat bath temperature T_b . At high temperatures the curves are the same for all cooling rates γ ; the system is still in equilibrium. At lower bath temperatures the system falls out of equilibrium and bends off the equilibrium curve. This bending is often associated with the onset

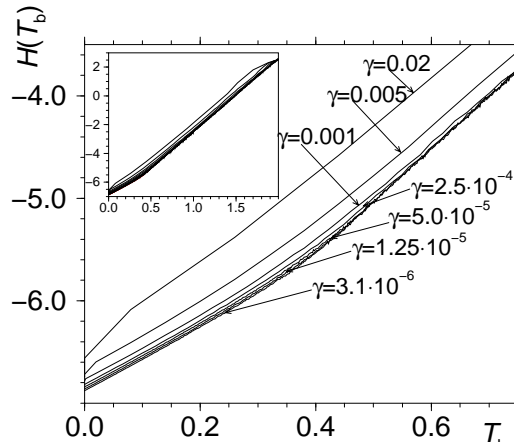


Fig. 1. Enthalpy H as a function of the heat bath temperature T_b . For clarity we show only every second cooling rate.

of the glass transition and occurs when the system relaxation time is approximately the inverse of the cooling rate. Therefore, faster cooling rates result in a higher temperature at which the system falls out of equilibrium.

To specify the temperature at which the system falls out of equilibrium we use the fictive temperature T_g proposed by Tool and Eichlin⁷. This is defined as the temperature at which the high and low T_b extrapolations of $H(T_b)$ intersect. Fig. 2 shows the cooling rate dependence of T_g , where, as expected, T_g decreases with decreasing cooling rate γ . Also included in the figure is a Vogel-Fulcher fit $T_g = T_0 + \frac{B}{\ln(A\gamma)}$, which provides with $T_0 = 0.348$, $A = 31.820$ and $B = 0.403$ a good fit to our data.

3.2. Resulting Glass at Zero Temperature

We now investigate the system after it has been cooled to zero temperature, i.e. the end configurations. Fig. 3 shows the radial distribution function of the A-particles. We find with decreasing cooling rate more pronounced peaks. The same effect is found in the bond-bond angle distribution (see Fig. 4). For the latter we used that two particles are defined to be neighbors and connected by a bond if their distance is less than the position of the first minimum of the corresponding (by particle type) $g(r)$. We find both for the radial distribution function and for the bond-bond angle distribution increasing order with decreasing cooling rate.

In the previous subsection we have seen that the system reaches a lower enthalpy with decreasing cooling rate. We now address *how* the system lowers its energy with decreasing γ . The question we ask is whether the system lowers its energy primarily by rearranging the particles and their neighbors or instead by the change in distances and bond-bond angles, as shown in Fig. 3 and Fig. 4. To answer this

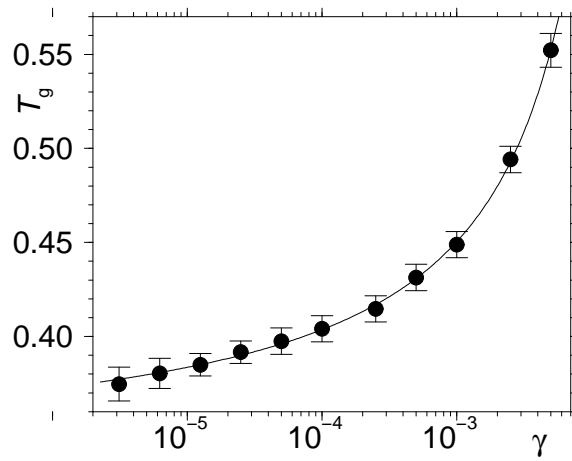


Fig. 2. Fictive Temperature T_g as a function of γ . Included is a Vogel-Fulcher fit.

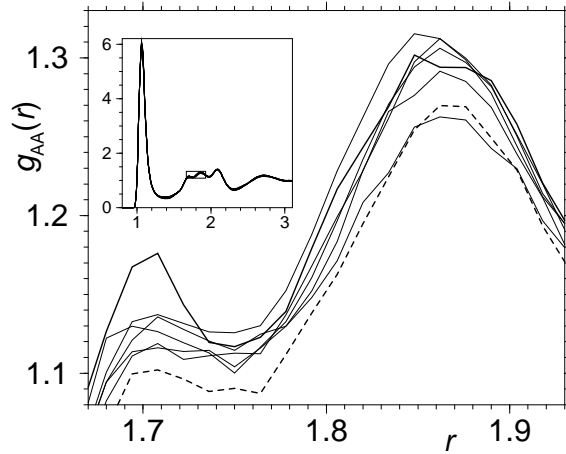


Fig. 3. Radial pair distribution for A-particles. The slowest/fastest cooling rate corresponds to the solid/dashed bold line. The figure shows an enlargement of the second nearest neighbor peak as indicated with a box in the inset.

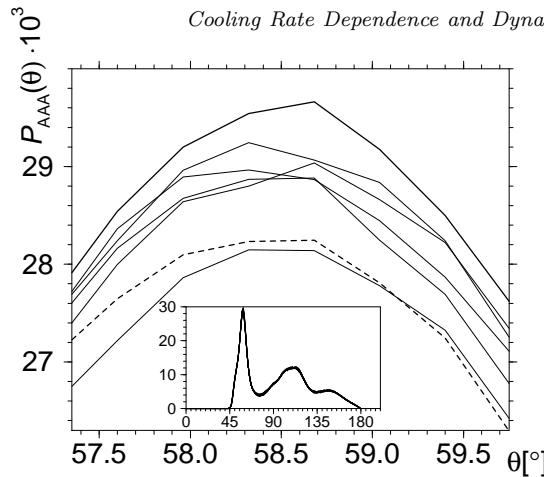


Fig. 4. Bond-bond angle distribution for A-particles. The slowest/fastest cooling rate corresponds to the solid/dashed bold line. The figure shows an enlargement of the first peak of the inset.

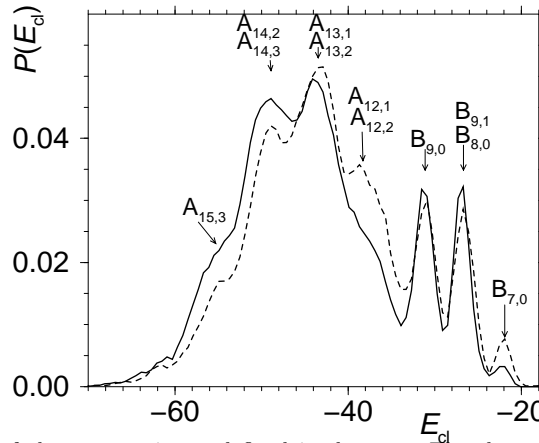


Fig. 5. Distribution of cluster energies as defined in the text. The slowest/fastest cooling rate corresponds to the solid/dashed bold line.

question we define a cluster as the set of a particle and its neighbors. We define a cluster type $\alpha_{\mu\nu}$ where the central particle is of type $\alpha \in \{A, B\}$ with μ nearest neighbors of which ν are of type B. The energy E_{cl} of a cluster is given by the sum of all pairwise interactions between any two members of the cluster. Fig. 5 shows the distribution of cluster energies and assigns the different cluster types to the corresponding peak positions. The distributions of the fastest and slowest cooling rate differ mainly in their peak height and only slightly in their peak position. We therefore can conclude that the energy is lowered primarily by a rearrangement of the particles.

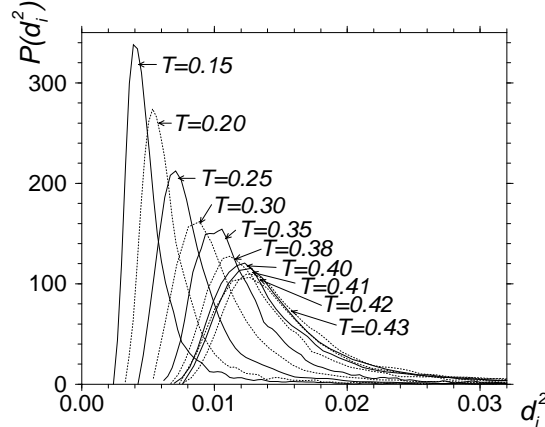


Fig. 6. $P(d_i^2)$ as defined in the text. The curves of all investigated temperatures are shown.

4. Melting: Dynamics Below The Glass Transition

Similar to the previous section we will again investigate the glass after it has fallen out of equilibrium. So far we studied static properties and in this section we will now investigate the dynamic properties of the glass below the glass transition temperature $T_c = 0.435$. This T_c corresponds to the glass transition temperature of mode coupling theory². Instead of cooling the system we are now asking the question how a glass melts.

Our initial configurations are obtained via a rapid quench to $T = 0.15$, starting from a well equilibrated temperature at $T=0.466$. We then continued in several steps. For each temperature we first equilibrated with 10^5 MD steps with a (NVT) simulation and then ran the production run of 10^5 MD steps with a (NVE) simulation. The volume is at all temperatures $V = 831$. Each equilibration and production run was followed by an instantaneous quench to the next higher temperature, where the process is repeated.

Having in mind the picture of an amorphous solid, we quantify the dynamics of a particle by its average fluctuations from its average position,

$$d_i^2 = \overline{\left| \vec{r}_i(t) - \overline{\vec{r}_i(t)} \right|^2} , \quad (4.1)$$

where the bar denotes an average over the whole time of the production run. Fig. 6 shows the distribution of d_i^2 of all particles from 10 independent runs and for all investigated temperatures. Most of the particles fluctuate around their average site with $d_i^2 \approx 0.01$, i.e. they are frozen into their positions and do not escape their cage of nearest neighbors during the whole production run. The larger the temperature the more is $P(d_i^2)$ shifted to the right.

We are interested in the fastest and slowest particles, hence we define mobile/immobile particles as the 5% with the largest/smallest d_i^2 . We study the spatial

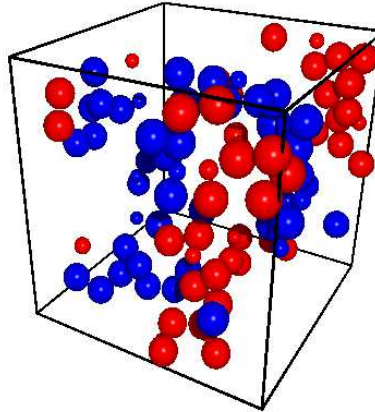


Fig. 7. Snapshot at $T = 0.15$ of the mobile A particles (large & light) and B particles (small & light) and the immobile A particles (large & dark) and B particles (small & dark).

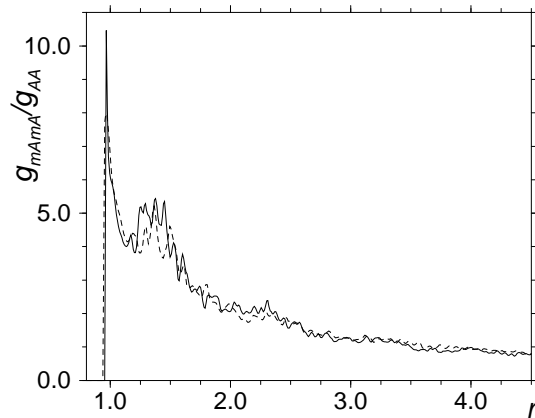


Fig. 8. g_{mAmA}/g_{AA} as explained in the text. The solid line corresponds to $T = 0.15$, the dashed line to $T = 0.43$.

distribution of these particles and also look at their surrounding in order to understand why they are more mobile or immobile.

4.1. Spatial distribution of Mobile and Immobile Particles

Fig. 7 shows a snapshot of the mobile and the immobile particles at $T = 0.15$ and time $t = 0$. We find similar snapshots at all other times and temperatures. The snapshot shows a clear heterogeneity. To quantify this heterogeneity we use, similar to Ref. [5], the ratio of the radial distribution function of mobile A-particles, g_{mAmA} , over that of all A particles, g_{AA} (see Fig. 8). We find similar results for all temperatures and also for the immobile particles. That the ratio g_{mAmA}/g_{AA} differs significantly from unity indicates a strong dynamic heterogeneity.

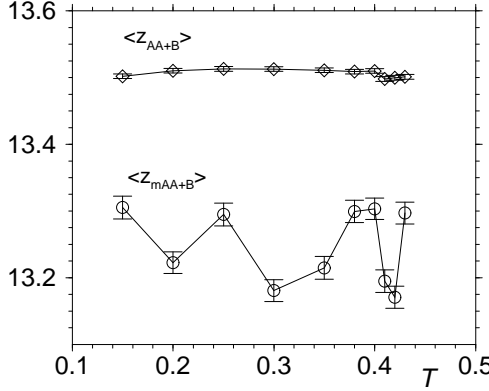


Fig. 9. Average total number of neighbors of a mobile A-particle ($\langle z_{mAA+B} \rangle$) in comparison with the total number of neighbors of any A-particle ($\langle z_{AA+B} \rangle$). The error bars correspond to the standard deviation of the mean. The real error bars are larger due to the lack of independent configurations over which the average has been taken.

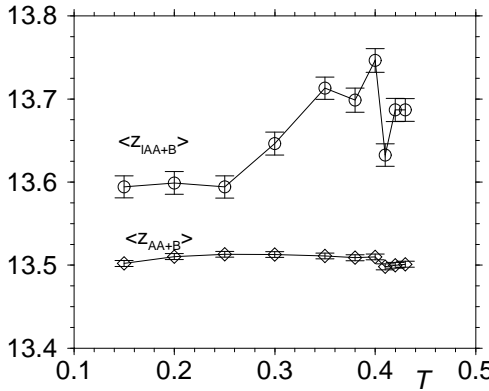


Fig. 10. Average total number of neighbors of an immobile A-particle, $\langle z_{lAA+B} \rangle$, in comparison with the total number of neighbors of any A-particle, $\langle z_{AA+B} \rangle$.

4.2. Neighborhood of Mobile and Immobile Particles

In this subsection we will investigate what causes a particle to be mobile or immobile. Fig. 9 shows a comparison of the average total number of neighbors of a mobile A-particle $\langle z_{mAA+B} \rangle$ and the average total number of all A-particles, $\langle z_{AA+B} \rangle$. We find that the mobile particle is on average surrounded by fewer particles than usual. Fig. 10 shows conversely that an immobile (localized) A-particle with average total number of neighbors $\langle z_{lAA+B} \rangle$ has more particles than usual surrounding it. The cage of mobile particles is less dense, the cage of an immobile particle is denser.

5. Conclusion

We investigated both the static properties of the configurations during and after the cooling to $T = 0$ and the dynamical properties upon the subsequent heating of a binary Lennard-Jones mixture. When cooling to $T = 0$ we find for all investigated quantities a cooling rate dependence; decreasing the cooling rate results in an increasing order and a decreasing enthalpy. The energetic part of the enthalpy is mainly lowered by a rearrangement of the particles. The fictive temperature is decreasing with decreasing cooling rate and is well fit by a Vogel-Fulcher law.

During the melting we find dynamic heterogeneity; the mobile and immobile particles are strongly clustered. The motion of particles appears to be determined by its neighborhood, as the average coordination number is decreased for mobile particles, indicating a looser cage, and increased for immobile particles.

Acknowledgment

K.V.-L. gratefully acknowledges financial support from Schott-Glaswerke, Mainz, and the SFB 262.

References

1. M. D. Ediger, C. A. Angell and S. R. Nagel, *J. Phys. Chem.* **B100**, 13200 (1996).
2. W. Kob and H.C. Andersen, *Phys. Rev. Lett.* **73**, 1376 (1994); *Phys. Rev. E* **51**, 4626 (1995); *ibid.* **52**, 4134 (1995).
3. K. Vollmayr, W. Kob and K. Binder, *J. Chem. Phys.* **105**, 4714 (1996); K. Vollmayr, Ph.D. thesis, University Mainz, 1995.
4. K. Vollmayr, W. Kob and K. Binder, *Phys. Rev. B* **54**, 15808 (1996).
5. W. Kob, C. Donati, S. J. Plimpton, P. H. Poole and S. C. Glotzer, *Phys. Rev. Lett.* **79**, 2827 (1997); C. Donati, J. F. Douglas, W. Kob, S.J. Plimpton, P.H. Poole and S.C. Glotzer, *Phys. Rev. Lett.* **80**, 2338 (1998); P. H. Poole, C. Donati and S. C. Glotzer, *Physica A* **261**, 51 (1998); S. C. Glotzer and C. Donati, *J. Phys.: Condens. Matter* **11**, A285 (1999); preprint cond-mat/9810060.
6. H. C. Andersen, *J. Chem. Phys.* **72**, 2384 (1980); J. R. Fox and H. C. Andersen, *J. Phys. Chem.* **88**, 4019 (1984).
7. A. Q. Tool and C. G. Eichlin, *J. Opt. Soc. Amer.*, **14**, 276 (1931).